

Theory and practice of elliptically bent x-ray mirrors

Malcolm R. Howells, MEMBER SPIE

Daniela Cambie

Robert M. Duarte

Steven Irick

Alasdair A. MacDowell

Howard A. Padmore

Timothy R. Renner

Lawrence Berkeley National Laboratory

Advanced Light Source

Berkeley, California 94720

E-mail: mrhowells@lbl.gov

Seungyu Rah

Pohang University of Science and

Technology

Pohang 790-784, Korea

Reubin Sandler

Lawrence Berkeley National Laboratory

Advanced Light Source

Berkeley, California 94720

Abstract. We report the results of our research and development in techniques for producing elliptical x-ray mirrors by controlled bending of a flat substrate. We review the theory and technique of mirror bending with emphasis on the optical engineering issues and describe our design concepts for both metal and ceramic mirrors. We provide analysis of the various classes of error that must be addressed to obtain a high quality elliptical surface and a correspondingly fine focus of the x-ray beam. We describe particular mirrors that have been built, using these techniques, to meet the requirements of the scientific program at the Advanced Light Source at Lawrence Berkeley National Laboratory. For these examples, we show optical metrology results indicating the achievement of surface accuracy values around and, in some cases, below $1\ \mu\text{rad}$ as well as x-ray measurements showing submicrometer focal spots. © 2000 Society of Photo-Optical Instrumentation Engineers. [S0091-3286(00)01410-0]

Subject terms: synchrotron radiation; elliptical cylinder; mirror; adaptive; x-ray; microprobe.

Paper 990303 received Aug. 2, 1999; revised manuscript received May 2, 2000; accepted for publication May 2, 2000.

1 Introduction

Substantial progress has been made in recent years in the fabrication of high-quality x-ray mirror surfaces by conventional grinding and polishing. One of the beneficiaries of this improvement has been the synchrotron radiation research community, which is faced with the task of building optical systems for the latest generation of synchrotron x-ray sources such as the Advanced Light Source at Lawrence Berkeley National Laboratory. The new sources have several orders of magnitude higher x-ray brightness than older machines, and they have enabled many new types of x-ray spectroscopy, microscopy and microanalysis to be performed. These experiments have generated a demand for reflective condensing optics of high light-gathering power and excellent focus quality and we have been involved in studies over several years to provide such optics for the beam lines at the Advanced Light Source (ALS). The mirrors of interest may be part of a prefocusing system that condenses the beam for some type of spectrometer or microscope or they may form a microprobe delivering the beam directly to a micrometer- or submicrometer-scale spot on the sample. The simplest focusing surfaces that can be used for these systems are spheres and circular cylinders, and these are adequate for some purposes. However, to obtain simultaneously the finest focus and greatest light-gathering power it is always advantageous to use elliptical cylinder mirrors. Naturally, the realization of this advantage depends on being able to construct the mirror with sufficient accuracy and we address that issue in various ways in what follows.

In this paper, we consider the technique of making elliptical cylinder mirrors by bending an initially flat plate.

We have adopted this approach over conventional rigid-mirror technology partly as a cost saving measure and partly in pursuit of a higher surface accuracy than could be achieved by zone polishing of a rigid substrate. Such advantages follow in part from the use of classical *flat* polishing. We also report some of our experiences in engineering and operating mirrors of this type, ranging from a 1-m-class condenser mirror to small microprobe optics delivering submicrometer-scale focal spots.

2 Scientific Motivations and Requirements

There are now microprobe or microfocus experiments in place at most of the third-generation synchrotron radiation laboratories.^{1,2} A variety of focusing techniques have been used as reviewed, for example, by Dhez. In selecting the one best suited to the microfocus experiments at ALS, particularly x-ray microdiffraction ($\mu\text{-XRD}$), fluorescence microanalysis ($\mu\text{-XRF}$) and x-ray photoelectron spectroscopy ($\mu\text{-XPS}$), we judged the need³ for convenient wavelength tuning to be a very high priority. This favors the methods based on specular reflection and we believe that, of these, the elliptical Kirkpatrick-Baez mirror scheme⁴ has the best flexibility and light-gathering power. In particular, either one or both members of the pair can be used for prefocusing or postfocusing with independent choice of magnification in the horizontal and vertical directions. We have now built and operated several elliptical Kirkpatrick-Baez systems and we discuss the performances achieved so far and projected for the future in the sections that follow. However, it is clear from the outset that, while a specular Kirkpatrick-Baez scheme is very competitive for tunability, light-gathering power and flux, it lags behind zone plates

with respect to spatial resolution by factors that range from about 4 for hard x rays to more than 10 for soft x rays.

Apart from high spatial resolution, the other principal requirement of the scientific applications is to not waste photons. This requires attention to the phase-space matching of the beam and the optical system and we discuss this further in Section 4.

3 Technical Approach and History

We are interested in bending a flat constant-thickness mirror by the application of unequal end couples. If the mirror has a constant width as well as constant thickness, then the result of such bending is a cubic curve which can be made to approximate an ellipse up to third order [see Equation 2)]. This enables correction of defocus and coma* while leaving higher order aberrations uncorrected. Higher order corrections to the bent shape are made, if required, by applying a controlled variation to the mirror width. Techniques of this general type have often been used before for both normal-incidence⁶ and grazing-incidence⁷⁻⁹ systems and have been quite widely used for focusing synchrotron radiation x rays.¹⁰⁻¹² This has included the use of bent metal mirrors with water cooling,¹³ gravity-corrected mirrors¹⁴ and directly deformable piezoceramic mirrors.^{15,16} The programmable-width concept was first introduced by Turner and Bennett¹⁷ and Underwood¹⁸ while the ALS group have developed a variable-thickness scheme in which the mirror and bending mechanism are built as a single monolith.^{19,20} The situation as of 1993 was reviewed by Howells and Lunt²⁰ and more recent work at the ALS^{2,21-24} and other third-generation light sources²⁵⁻²⁷ is now on record.

Some of the mentioned mirrors have achieved their specified performance levels, while others have failed due to the application of unintended additional forces. The difficulty of applying the couples with sufficient accuracy is increasing at the present time due to the smaller focal spots that are being sought. In this paper, we describe some new ways to apply the couples via weak leaf springs. This approach makes it much simpler to control the amount of bending with high accuracy and also lends itself to schemes that do not apply tensile forces to the mirror. We concentrate specifically on elliptical mirrors, although the methods of construction we will discuss are also applicable to the quadratic (i.e., circular) and cubic approximations to the ellipse.

4 Phase Space Acceptance of a Grazing Incidence X-Ray Mirror

Let us consider the quantitative effect of phase-space limitations, which apply to all focusing systems, including x-ray mirrors. Suppose a mirror is required to focus light from a source of full width s at distance r to a spot of width s' at distance r' . The useful angles of grazing incidence lie in the range zero to θ_c (the critical angle) so, in principal, the convergence angle for the beam arriving at the focus

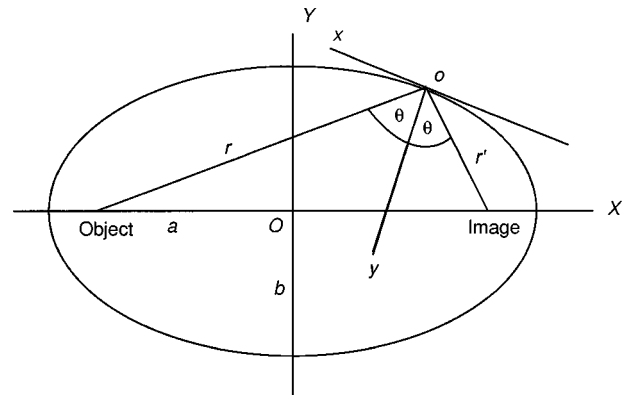


Fig. 1 Ellipse layout and notation.

could be up to $2\theta_c$. However, in practice one can never make the mirror long enough to cover such a large range of angles and the limit is set by the r' values and the geometry of fitting in both mirrors of the pair. Roughly speaking, this limits the mirror lengths to about r' and the convergence angle to about $\theta_c/2$. If the source angle is ϕ and the focused beam angle is ϕ' , then $s\phi = s'\phi'$ and the usable radiation emission angle is given by $\phi = s'\theta_c/(2s)$. For example, the size $s_H \times s_V$ of an ALS bending-magnet source is $240 \times 20 \mu\text{m}^2$. Therefore at 10 keV ($\theta_c \approx 6 \text{ mrad}$), with a $1\text{-}\mu\text{m}$ focused spot, 0.15 mrad of the vertical and 0.013 mrad of the horizontal fans emitted by the source would be usable. This shows that almost all of the vertical fan can be used, which is a benefit of the high vertical brightness. On the other hand, a smaller fraction of the horizontal fan can be used implying that the horizontally focusing mirror will normally be the shorter and therefore the downstream member of the pair. Some further examples of this type are given by Howells and Hastings.²⁸

The broad picture is that microprobe mirrors have rather small usable emission angles and utilize only a limited portion of the beam available at a bend magnet port. On the other hand, condenser mirrors are usually required to deliver a larger spot (the size of an entrance slit or sample typically) and can usually accept the entire beam. Consequently microprobe mirrors are typically much smaller than condensers. In the case of a microprobe, the figure of merit is the resolving-power-phase-space-acceptance product. The resolving power is proportional to $1/s'$ and the acceptance is $s'\phi'$. The figure of merit thus reduces to ϕ' , or equivalently to the mirror size that indicates that microprobe mirrors should be made as large as possible up to the limit set by the usable emission angle.

5 Geometrical Considerations

An elliptical cylinder mirror is defined by the optical parameters r, r' and θ and has major and minor semiaxes a and b and eccentricity e (see Fig. 1). It is represented in the X - Y coordinate system by

$$\frac{X^2}{a^2} + \frac{Y^2}{b^2} = 1. \quad (1)$$

*It has been pointed out by Underwood⁵ that the term coma should not be used to describe this aberration and that certain errors beyond mere semantics can result from so doing. However, the usage has become so widespread that it is now conventional. Thus we follow the convention in this work.

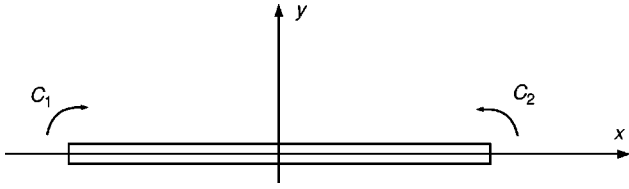


Fig. 2 Notation for discussing beam bending using two different couples.

The same ellipse can also be represented by a power series in the x , y coordinates of Fig. 1 as follows:

$$y = a_2 x^2 + a_3 x^3 + a_4 x^4 + \dots, \quad (2)$$

so that the slope and curvature are,

$$\frac{dy}{dx} = 2a_2 x + 3a_3 x^2 + 4a_4 x^3 + \dots \quad (3a)$$

$$\frac{d^2 y}{dx^2} = 2a_2 + 6a_3 x + 12a_4 x^2 + \dots \quad (3b)$$

The a_i coefficients for the ellipse are given up to a_{10} in the Appendix.²⁹ Each term $a_i x^i$ of the series in Equation (2) corresponds to an aberration of the reflected wave front which will be corrected if the term is faithfully built into the mirror shape. The $i=2$ term corresponds to defocus, the $i=3$ one to coma (see earlier footnote) [linear variation of curvature with position in the aperture (see Equation (3))], the $i=4$ one to spherical aberration and so on.

The major and minor semiaxes a and b , the eccentricity e of the ellipse, the coordinates (X_0, Y_0) of the pole of the mirror and the angle δ between the OX and ox axes are related to the optical parameters r, r' and θ by the following relations:

$$\begin{aligned} 2a &= r + r', & Y_0 &= \frac{rr' \sin 2\theta}{2ae}, \\ (2ae)^2 &= r^2 + r'^2 - 2rr' \cos 2\theta, & |\delta| &= \cos^{-1} \left(\frac{\sin \theta}{e} \right), \\ b^2 &= a^2(1 - e^2), & X_0 &= \pm a \sqrt{1 - \frac{Y_0^2}{b^2}}, \end{aligned} \quad (4)$$

where the square root is $+$, zero or $-$ according as $r >$, $=$ or $< r'$.

6 Formation of an Elliptical Surface by Beam Bending

First consider a beam that is being bent by the action of two end couples C_1 and C_2 , defined to be positive in the sense drawn in Fig. 2. One can show that the bending moment will vary linearly from C_1 at $x = -L/2$ to C_2 at $x = +L/2$. The differential equation for the shape of the bent beam is the Bernoulli-Euler equation³⁰ that here takes the following form,

$$EI_0 \frac{d^2 y}{dx^2} = \frac{C_1 + C_2}{2} - \frac{C_1 - C_2}{L} x, \quad (5)$$

where E is Young's modulus, and I_0 is the moment of inertia of the beam cross section, considered for the moment to be constant.

To make the cubic approximation to the ellipse, we equate coefficients of the constant and linear terms of Equations (3b) and (5) to determine C_1 and C_2 .

$$\frac{C_1 + C_2}{2} = 2EI_0 a_2 = \frac{EI_0}{R_0}, \quad (6)$$

$$\frac{C_1 - C_2}{L} = -6EI_0 a_3 = -\frac{3EI_0}{R_0} \frac{\sin \theta}{2} \left(\frac{1}{r'} - \frac{1}{r} \right), \quad (7)$$

where R_0 is the radius of curvature at the center. Thus the mirror will match the ellipse up to third order if the *bending moment* is equal to C_1 and C_2 at $-L/2$ and $+L/2$. The actual couples applied to the mirror need not be positioned exactly at $-L/2$ and $+L/2$ and in fact they are best placed somewhat further from the mirror center to allow for the effect of end errors (see Fig. 6 in Section 9.1.3). To make the quadratic approximation, we would set the magnitude of both couples equal to $C = EI_0/R$. The cubic approximation that we have defined here is not the only possible one. We discuss later in Section 9.2.2 how it can be improved in the case that externally induced spherical aberration is present. The optimum approximation to a parabolic mirror has been discussed by Underwood.¹⁸

A better solution is often to construct a nominally exact elliptical shape. We can do this by modifying the width of the mirror so that I_0 in Equation (5) becomes $I(x)$ and is calculated to give the right radius of curvature at each value of x as specified by Equation (5). We could do this for almost any pair of end couples but as an example we use the ones given by Equations (6) and (7). Inserting Equations (3), (6) and (7) into Equation (5) and remembering that $I = bh^3/12$, where b and h are the width and thickness of the mirror, respectively, we obtain an expression for the width needed to produce the desired elliptical shape:

$$b(x) = \frac{b_0(1/R_0 + 6a_3 x)}{2a_2 + 6a_3 x + 12a_4 x^2 + \dots}. \quad (8)$$

In this expression we have expressed the ellipse curvature according to Equation (3) which is simpler and sufficiently accurate for almost all purposes if the series is taken up to tenth order as in the Appendix. However, it is also straightforward to calculate an exact value based on Equation (1).

7 Range of Validity of the Quadratic and Cubic Approximations

The quadratic approximation corresponds to building $y = a_2 x^2$ and the cubic approximation to building $y = a_2 x^2 + a_3 x^3$. To investigate the range of validity of these approximations, we made a calculation³¹ in which the length of the circular or cubic mirror is allowed to extend in each direction until the slope error relative to the corresponding

Table 1 Some bent mirrors made at the ALS.

	μ -XPS (Horiz.)	μ -XPS (Vert.)	PEEM Condenser	7.3.3 Condenser	μ -XRD (Vert.)	μ -XRD (Horiz.)
Initial shape	Flat	Flat	Flat	Cylinder, radius 87.1 mm	Flat	Flat
Final shape	Elliptical cyl.	Elliptical cyl.	Elliptical cyl.	Toroid	Cubic cyl.	Elliptical cyl.
r (m)	4	3.88	20	16	30.6	31
r' (m)	0.1	0.22	1.85	16	0.5	0.1
Grazing angle (deg)	1.6	1.6	2.5	0.31	0.33	0.33
Clear aperture (mm ²)	60×25	110×38	1010×100	600	163×42	40×10
Thickness (mm)	3	6.7	15	32	9.52	4
Min-max bending radius (m)	4.5, 9.7	10, 20	49, 107	2963	130, 211	28, 40
Achieved root mean square (rms) slope error	2	3	3 (60% aperture) 14 (100% aperture)	1.0	1.4	0.6
before bending (μ rad)						
Achieved finish (\AA rms)	3.0	4.0	7	7.2	<1	5
Measured x-ray spot size FWHM (μ m)	1.0	1.2	30 (100% aperture)	50	0.8	0.4*
Material	17-4 PH stainless steel	17-4 PH stainless steel	Mild steel (1006)	Silicon	ULE	ULE
Polisher	Dallas Optical Systems	Dallas Optical Systems	Boeing North American	Frank Cook	General Optics	Boeing North American
Attachments	Nut and bolt	Nut and bolt	Nut and bolt	Glue	Glue	Glue
Special challenges	Extreme curvature		Avoid tension, large size	Figure accuracy		Figure accuracy

*See Section 11.3 for comments on the ultimate performance of this mirror.

ellipse reaches a prescribed value Δ . This means 2Δ is roughly the peak-to-valley slope error. On this basis, the permitted mirror full lengths L_2 and L_3 for the quadratic and cubic approximations respectively are determined to be

$$L_2 = k_2 r' \left(\frac{\Delta}{\theta_G} \right)^{1/2} \quad (M \leq 0.5) \quad L_3 = k_3 r' \left(\frac{\Delta}{\theta_G} \right)^{1/3} \quad (M \leq 1), \quad (9)$$

where M is the magnification; θ_G is the grazing angle, and k_2 and k_3 are dimensionless constants with values 3.28 and 2.97, respectively. Evidently the approximate mirror shapes will work better for harder x-ray mirrors because of their smaller θ_G values. With an appropriate choice of Δ , the approximate mirrors can achieve arbitrarily small spot sizes (provided they are sufficiently well made). However, their aperture will be limited according to Equations (9) and for the smallest spot sizes, the loss of phase-space acceptance compared to a true ellipse will be severe.

To illustrate how much light-gathering power is lost by approximating the ellipse, we consider the hard-x-ray μ -XRD mirror at the ALS as an example. Taking the ellipse length as r' and using Equations (9) with a 1 μ m spot size and the μ -XRD parameters in Table 1, we find that horizontally, the limits on the lengths of the ellipse, cubic and circle mirrors are 100, 22 and 7 mm, respectively. Vertically, the same three limits are 500, 66 and 15 mm and the concentration factor (of the beam area) for the ellipse, cubic and circle cases would be 1.7×10^6 , 5.0×10^4 and 3.5×10^3 , respectively. Even larger losses of x-ray flux are found if elliptical mirrors are replaced by their approxima-

tions in soft x-ray microprobe schemes. However, note that the values given by Equation (9) do not take into account the possibility of aberration balancing which we discuss later in Section 9.2.2.

8 Mirror Bending by Weak Leaf Springs

8.1 Mechanical Principles

We consider here two types of bending machines: those which put the mirror in tension and those which do not. Example implementations of the two classes of leaf-spring bending mechanisms (with and without the tensile force) are shown in idealized form in Fig. 3.

To understand the statics of the arrangement in Fig. 3(a) suppose the loading is applied in two steps:

Step 1. The force F is applied by moving the slide to the left. This applies couples of equal magnitude and *opposite* sense at the mirror ends while the axial forces in the springs remain equal to zero. The magnitude (C) of the couples is $Fl/2$ if the springs are rigidly clamped at the base as shown. (It would be Fl if they were hinged.) To obtain couples of equal magnitude it is only necessary that the springs be equal in length. It is not necessary that they be elastically identical.

Step 2. The force G is applied at the right end of the mirror. This applies couples of the *same* sense at the mirror ends and induces axial forces in the springs which are equal in magnitude and opposite in sign, the one in the right

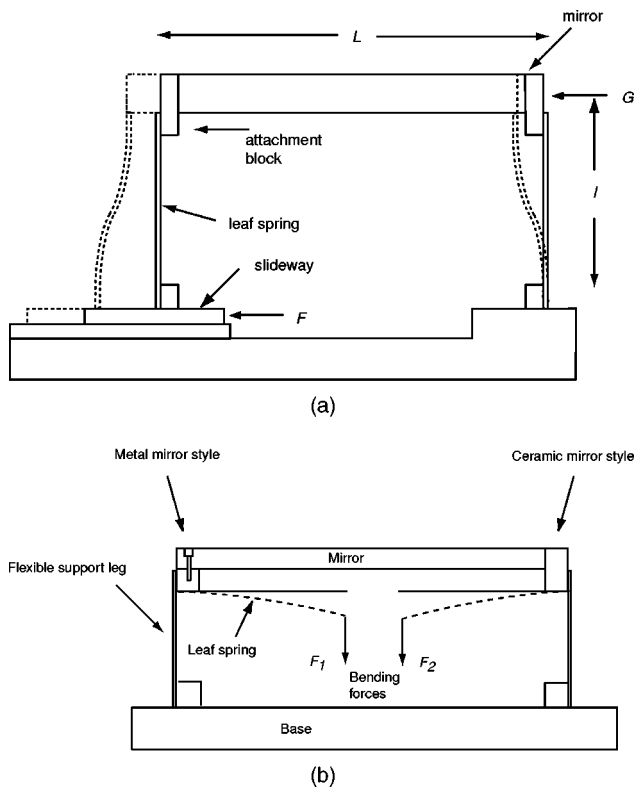


Fig. 3 (a) An “S” spring bender in which equal and opposite couples are applied by moving the slideway to the left (force F), while couples of the same sign are applied by pushing the whole mirror to the left (force G). (b) Avoids the mirror tension implicit in (a) by applying the couples by means of forces transverse to the mirror. The latter scheme has also the advantage of being all-flexural.

spring being tensile. The magnitude (ΔC) of the applied couples is $Gl/4$ and that of the axial forces is $GL/2l$.

The net effect of these two steps is that couples of magnitude $C + \Delta C$ and $C - \Delta C$ are applied at the right and left ends of the mirror, respectively. The value of C , the mean of the two couples, determines the center radius of the mirror [Equation (6)]. The value of ΔC determines the amount of coma correction [Equation (7)].

The advantages of this type of design are as follows:

1. The focal length of the mirror and the amount of aberration correction are *independently* adjustable using F and G .
2. The springs are made *weak* so that small deformations of the mirror are produced by large, easily controllable, movements of the drivers.
3. The use of a prescribed driving force, rather than a prescribed displacement, enables manufacturing errors or changes in the mirror size (due to thermal expansion for example) to be tolerated as long as they are small compared to the driver motion needed to bend the mirror.
4. The forces are applied relative to a rigid base. (Some simplifications can be obtained by making this base part of the vacuum envelope.)

The bending system shown in Fig. 3(b) is a variant that does not put the mirror in tension. It has the virtue of simplicity although it lacks the separation of focusing and aberration correction. Otherwise it shares most of the features of the “S” spring system.

Both of these schemes are being used for mirrors at the ALS. The “S” spring type is being used for μ -XRD while the XPEEM condenser is roughly of the second type. The μ -XPS system uses a variant of the “S” spring scheme, in which the springs are hinged at the bottom and therefore bend in the manner of a cantilever. In Section 11, we give further discussion of the performance of these designs in practice.

8.2 Fabrication Methods

We believe that the guiding considerations in substrate manufacture should be dimensional stability³² (in particular low residual stress), and the flatness and parallelness of the front and back surfaces. (Note that curvature *is* an error in an elliptical bender.) These requirements favor construction as a simple flat plate and use of standard machining-grinding-lapping sequences to achieve high quality surfaces on both sides. Both standard stress relief and thermal cycling may be required according to the choice of material³² as described for specific cases in Section 11. As we discuss in the section on antistatic bending (Section 9.1.2), the quality of the back surface is important and may determine the distortion due to the joint between the mirror and the bender. The lapping step is a low-stress procedure that is required both for surface quality and to remove the stressed surface layer due to the preceding grinding step. (It is noteworthy that after lapping it becomes possible to measure the shape using the long trace profiler.) By these methods, it should be possible to get most mirrors flat and parallel within about a part in a thousand. The most likely errors are curvature and wedge, which we treat quantitatively in Section 9.4.

The calculated shape of the edges [Equation (8)] should be cut early on in the process by numerically controlled (NC) milling in the case of metal substrates or NC grinding in the case of ceramic ones followed in both cases by suitable stress relief. NC machines are less readily available for ceramics and it is sometimes sufficient to utilize a polygon shaped mirror as a compromise between a constant-width and the exact calculated curve. The advantage of the polygon is that it can be cut with a saw.

A different form of correction by edge shaping was practiced by Lienert and coworkers³³ who modified the edges of their bent-crystal optics after the optics had been manufactured so as to improve the shape of the Bragg planes. The errors were due to alteration of unavoidable stresses when the silicon was cut to shape and the corrections were based on point-by-point x-ray-reflection measurements of the optics. This has not yet been done with a bent mirror. However, we do have evidence that some fused silica mirrors can be shaped after polishing without much damage to their optical figure. This provides some hope that such mirrors might be similarly corrected on the basis of optical measurements made after polishing and bending.

8.3 Assembly

A major step is the making of the joint between the mirror and the bending mechanism. We discuss this later in connection with potential errors due to adhesive or nut-and-bolt joints (Section 9.1.2) and with the technique for strong adhesive joints (Section 10). Once the joints to the mirror ends are made, the rest of the assembly process is usually a nut-and-bolt operation in which the difficult step is the last one that closes the loop made by the mirror and the bending machine. Often the assembled mirror has a twist greater than the sagittal slope error tolerance. It is then important that some part of the assembly should be deformable or adjustable with sufficient resolution to reset the twist within tolerance. There are various ways to measure the twist when making this setting. A convenient one that we have used is to make separate autocollimator readings at the ends of the mirror, each time aligning the instrument with respect to the vertical by means of a tilt meter.³⁴

8.4 Optical Testing

Once the mirror can be bent, the task of setting the bending couples to the best values, as measured by the long-trace profiler, can begin. When the x-ray source is of rms size Σ at distance r , the allowed rms slope errors (σ), as measured by the long trace profiler, are usually defined as follows.

Tangential plane: $\sigma_t \leq \Sigma_t / (4r)$,

Sagittal plane: $\sigma_s \leq \Sigma_s / (4r \sin \theta_G)$,

where θ_G is the grazing angle. These are useful practical definitions that are intended as the condition to not degrade the source brightness. However, they are simplistic and do not provide any guarantees of performance. Moreover, the σ_t values corresponding to a third generation x-ray source at a few tens of meters distance are often beyond the state of the art of mirror making ($\sigma_t < 0.1 \mu\text{rad}$ for example). The procedure to get the best values of the bending couples has been discussed by Rah et al.²⁹ It is noteworthy that one can usually do much better than simply selecting the values that satisfy Equations (6) and (7), as discussed in Section 9.2.2.

9 Analysis of Errors in Mirror Benders

The practical implementation of high-quality bendable mirrors is largely a question of analyzing and controlling the errors that can produce departures from the ideal elliptical-cylinder surface that we are seeking to create. We now give a detailed analysis of the following classes of error.

1. intrinsic errors that exist even for perfectly made and operated mirrors
2. errors produced by environmental effects
3. operation of the mirror at other than its design conjugates
4. manufacturing errors

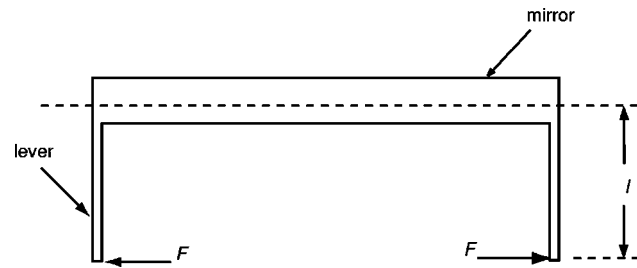


Fig. 4 Schematic of a type of mirror bender that puts the mirror in tension.

9.1 Intrinsic Errors

9.1.1 Tension effects

The design shown schematically in Fig. 4, which is commonly used, applies a tensile force to the mirror which will tend to have a straightening effect and we now proceed to calculate the size of the resulting error. To do this consider a simplified case of a circularly-bent mirror with equal couples, applied by forces F and bending levers of length l , at the ends of the mirror (Fig. 4). This leads to $C_1 = C_2 = Fl$ and the mirror is subjected to a tensile force F . Allowing for the latter, Equation (5) becomes^{35,36}

$$\frac{d^2y}{dx^2} - q^2y = q^2l \quad \text{where} \quad q = \sqrt{\left(\frac{F}{EI_0}\right)} \quad (10)$$

leading to a slope distribution

$$\frac{dy}{dx} = \frac{x}{R_0} \left(\frac{\sinh qx}{qx} \right). \quad (11)$$

The first term in Equation (11) x/R_0 is the slope distribution of the correct circular curve while the term in the square brackets is an error term caused by the tensile force F . When F tends toward zero, the error term tends toward unity. The error is most damaging for long mirrors with steep curvature and short bending levers. For example with $L = 1 \text{ m}$, $l = 0.05 \text{ m}$, $R_0 = 100 \text{ m}$, the maximum slope error would be 16 arcsec. For the majority of practical cases, however, the error is likely to be negligible ($< 0.1 \mu\text{rad}$, say).

9.1.2 Anticlastic bending effects

The design scheme described in this article is essentially a beam-theory concept so we should be alert for situations where beam theory may be expected to break down. Such a case arises when the mirror width is not small compared to its length and the mirror needs to be treated as a plate. One has then to take into account the fact that, in the absence of boundary conditions, the “natural” sagittal curvature will be equal to ν times the externally applied tangential curvature (ν being Poisson’s ratio). The degree to which this “anticlastic” curvature can be removed by constraining the two nominally straight edges to remain exactly straight has been analyzed by Ferrer and coworkers³⁷ in connection with focusing crystals. Consider a plate of length a and

width b bent into a circular cylinder by equal and opposite couples applied to the edges $x=0$ and $x=a$, which are assumed to be clamped straight. The x and y axes are defined so that the edges of the plate are $x=0$, $x=a$ and $y = \pm b/2$. It can then be shown^{38,39} using the standard methods of plate theory,⁴⁰ that the closed-form solution for w (the out-of-plane displacement) is as follows.

$$w = \sum_{m=1}^{\infty} \left(\frac{4a^2}{R\pi^3} \frac{1}{m^3} + A_m \cosh \frac{m\pi y}{a} + B_m \frac{m\pi y}{a} \sinh \frac{m\pi y}{a} \right) \sin \frac{m\pi x}{a}, \quad (12)$$

where R is the nominal bending radius, $m=1, 3, 5, \dots$ and

$$A_m = C_m [\sinh \alpha_m (1 + \nu) - \alpha_m \cosh \alpha_m (1 - \nu)]$$

$$B_m = C_m \sinh \alpha_m (1 - \nu)$$

$$C_m = \frac{4a^2 \nu}{R\pi^3} \frac{1}{m^3} \frac{1}{\sinh \alpha_m \cosh \alpha_m (3 + \nu) (1 - \nu) - \alpha_m (1 - \nu)^2}$$

$$\text{and } \alpha_m = \frac{m\pi b}{2a}.$$

The first term of this solution is the Fourier series of the intended cylindrical shape and the other terms represent the errors due to anticlastic bending. Such errors can become important for mirrors with large widths and/or large grazing angles.

Another type of anticlastic-bending effect may appear when a glass or silicon mirror substrate is glued to the metal plate that is used for attaching the bending mechanism. An important factor to consider in this case is the fractional shrinkage ε_G of the glue. First we consider the effect of shrinkage of the glue layer *in its own plane*. Suppose we are joining two plates of thickness, elastic modulus and Poisson's ratio h_1 , E_1 , ν_1 and h_2 , E_2 and ν_2 , respectively. Suppose further that the glue layer behaves elastically and has thickness h_G ($\ll h_1, h_2$) and modulus E_G . It can then be shown that the stress due to shrinkage induces a spherical radius R_G given by

$$R_G = \frac{E_1 h_1^2}{6(1 - \nu_1) \varepsilon_G E_G h_G} \frac{1 + 4en + 6en^2 + 4en^3 + e^2 n^4}{1 - en^2}, \quad (13)$$

where $n = h_2/h_1$ and $e = [E_1/(1 - \nu_1)]/[E_2/(1 - \nu_2)]$. In the special case that $n \rightarrow 0$, which represents a single plate with a thin coating, the second fraction on the right is equal to unity and Equation (13) reduces to the Stoney equation.⁴¹ Now, in practical cases (glue thickness about 50 to 150 μm), the cross section of the glue layer will be much smaller than that of the two plates that are being joined. Therefore the shrinkage forces due to the glue layer are not likely to produce a large distortion. Nevertheless, at the microradian level, this is still something to keep in mind. Up to now there is no anticlastic effect due to the glue.

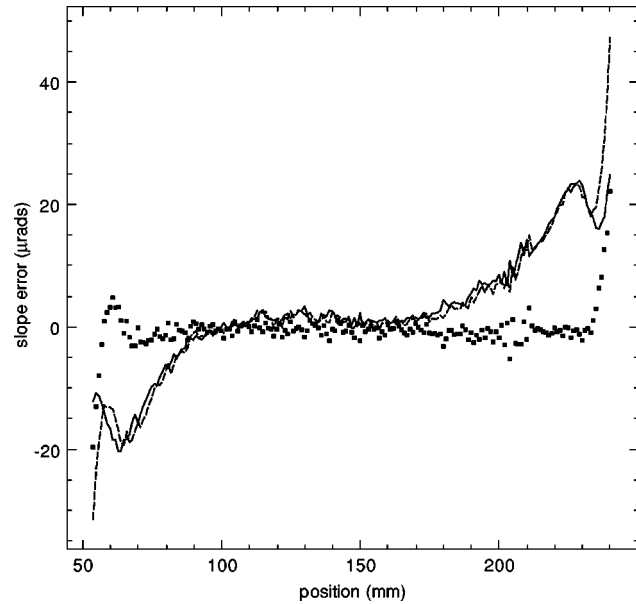


Fig. 5 Surface shape of a rectangular development mirror with a bending mechanism of the type shown in Fig. 3(a) except that here the steel end fixtures were glued to the backside. The $9.5 \times 42.5 \times 200 \text{ mm}^3$ mirror was fabricated from fused silica with an initial rms flatness error of less than $1 \mu\text{rad}$. The solid line represents the unbent state, the dashed one a bent radius of 151 m and the dotted line the difference. Tilt, piston and curvature have been removed from both. The close agreement of the bent and unbent curves indicates that the serious errors at the ends of the mirror are not due to bending but rather to the method of attaching the end fixtures.

On the other hand, consider the shrinkage of the glue layer in a direction *perpendicular to its own plane*. In this case, the cross section involved (the joint area) is large, and the shrinkage force will normally be dominant compared to the flexural forces of the two plates that are opposing it. We first became interested in this issue when we made long-trace profiler tests on a glass mirror, with steel fixtures glued on its underside. We observed the unexpected slope errors (shown in Fig. 5) extending a distance equal to five or six times the thickness beyond the glued area and taking about half of the mirror out of tolerance. Our first thought was that a tangential curvature, due in some way to the joint, might produce such a long-range error. However, insight based on St. Venant's principal, which was confirmed by finite-element analysis, indicated that the effects of such distortions in the tangential plane would normally extend only about one thickness beyond the region of the joint.

We now believe that the errors arise in a more indirect way as follows. Suppose the curvatures of the two surfaces being joined by the glue are miss matched. The glue layer would then be non uniform, and, after shrinking in proportion to its thickness, would induce both a tangential and sagittal curvature of the mirror in the joint area. The tangential curvature would be ineffective, as noted above, but the *sagittal curvature* of the glue-joint would continue far beyond the joint area and would produce a corresponding anticlastic tangential curvature as seen in Fig. 5. This picture is made plausible by finite-element analysis which shows that a mirror with back-glued metal blocks of suitable curvature can reproduce Fig. 5 almost exactly.

The message of this is to avoid such sagittal distortions

at the ends of the mirror. This is equally important for bolted or glued joints to the back (or front) of the mirror. It appears that VUV and soft x-ray mirrors with their high curvature and corresponding low thickness are particularly vulnerable to this type of error. If the mirror is thicker than about 0.5 cm, then the fixtures can be glued to the end and in our experience this is one way to eliminate the problem. For hard x-ray mirrors, typically having lengths up to a meter and radii of at least a kilometer, one normally makes the thickness much greater (5 to 10 cm) to resist bending under gravity and in these cases the distortions due to end attachments are much less of a problem. We give an illustration of bending a beam of this general shape in the next section.

9.1.3 Line and strip loading of the mirror surface by clamps

In several traditional bender designs, the end couples are applied to the mirror by four rods in a four-point-bending configuration.⁴² This delivers a line loading to the mirror surface. The surface slope at distance x along a line perpendicular to the line load can be calculated in plane strain if the mirror is idealized as a 2-D elastic half plane.⁴³

$$\text{slope} = (1 - \nu^2) \frac{2P}{\pi E} \frac{1}{x} \quad (\text{line load}), \quad (14)$$

where P is the load per unit length. If the load is applied over a finite area of width $2a$, roughly representing a flat clamp, the effect can be obtained by integration⁴³ of Equation (14).

$$\text{slope} = \frac{2(1 - \nu^2)p}{\pi E} \ln \left(\frac{x+a}{x-a} \right) \quad (\text{strip load}), \quad (15)$$

where p is the load per unit area. We compared both of these equations to finite-element analysis of mirrors of thickness 1 cm with realistic bending loads. The agreement was good and, furthermore, the slope errors fell to values much less than a microradian within 1 cm of the loaded area. This suggests that bender designs using clamps acting perpendicular to the mirror surface can, in principle, be effective. As an illustration of these types of calculation we show both the measured and calculated 2-D stresses in the four-point-bender geometry as given in a classical text on photoelasticity⁴⁴ (Fig. 6).

9.2 Errors Produced by Environmental Effects

The environmental influences that impact synchrotron radiation optics are mainly the vacuum, the thermal changes due to illumination by the beam and gravity. Here we consider only the last two.

9.2.1 Temperature

If the mirror expands more than the base then one can see from Figs. 3(a) or 3(b) that the result will be unintended end couples tending to make the mirror more convex. The slope errors at the ends produced by such couples are $3\alpha e i L^2 / 2EI l^2$ radians/°C where E , I , L and e , i , l are the modulus, section moment and length of the mirror and support legs, respectively. To ensure that these slope errors are

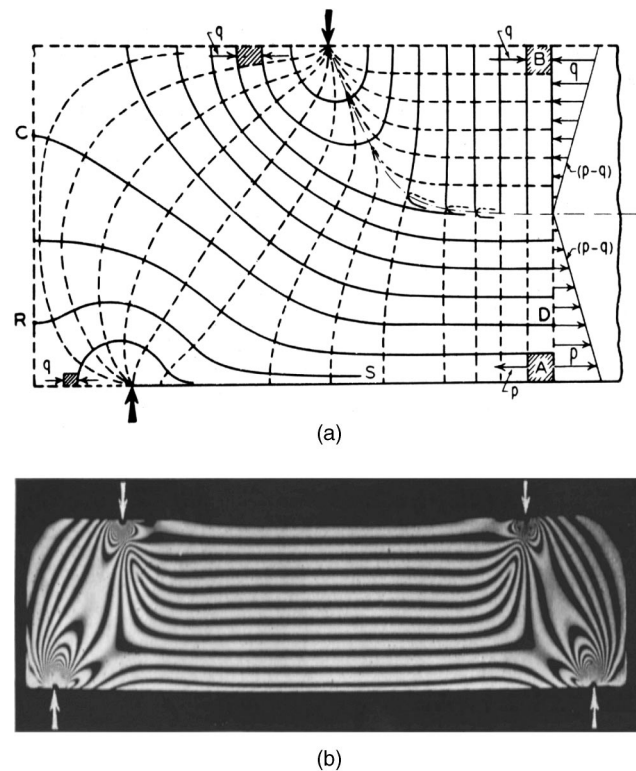


Fig. 6 Theory-of-elasticity calculation in plane stress (a) and photoelastic measurement (b) of the stress pattern due to four-point bending of a uniform beam.⁴⁴ Note that the pattern of purely longitudinal stresses that one expects for a circularly bent beam is not established until about one thickness away from the applied point loads that produce a locally nonideal stress pattern.

negligibly small, we have to make the legs sufficiently flexible within the limitation that the loading should not approach the critical force for buckling, which in this case is $\pi^2 e i / l^2$. This is generally easy to do.

9.2.2 Gravity

When a mirror of uniform cross section, simply supported at its ends, sags under gravity, it assumes a symmetrical shape of the general type $y = ax^2 + bx^4$, which represents a mixture of defocus and spherical aberration. Under the influence of gravity alone a and b take the values $a_0 = mL^2/16EI$ and $b_0 = -m/24EI$, where m is the weight per unit length. This shows that the slope error at either end due to defocus is three times larger than that due to spherical aberration and in the opposite direction so that the net end slope error is twice that due to the spherical aberration. For convenience we adopt the magnitude of the spherical aberration end slope as a reference “unit.” For a uniform mirror under gravity alone the size of the unit is $-mL^3/48EI$. For “rigid” mirrors one can remove much of the distortion by choosing the best spacing between the support points. An analysis of this choice has been given by Howells and Lunt,²⁰ who show that the minimum gravitational peak-to-valley slope error is achieved with a spacing of $L/\sqrt{3}$, which gives a factor 16.4 improvement in the end slope error compared to having the supports at the ends. Other approaches to eliminating the unwanted effects of

gravity are an increase in I/m (for example, by an increase of the depth), the use of high-specific-strength materials such as beryllium or silicon carbide or active correction by a series of springs.¹⁴

The situation is different if the mirror has adjustable end couples. Then the value of a becomes controllable but the value of b does not. This certainly implies that the curvature can be removed leaving one unit of end slope error. However, there are still two more strategies for reducing the spherical aberration, both of which are quite effective. The first is to intentionally defocus the system which is a classical form of aberration balancing.⁴⁵ It works for all types of spherical aberration whether the source is manufacturing error, gravity or the use of an ellipse at other than its design conjugates. It can be shown⁴⁶ that, for gravitational distortion, the best peak-to-valley slope error is obtained by setting $a = -3bL^2/8$, which reduces the end slope to 0.25 units. Similarly the best rms slope error requires $a = -3bL^2/10$ and is equal to 0.076 units. The process of finding these optimum settings is not as difficult as it may seem. For example, the rms-slope-error optimum is found automatically if the mirror focal length is tuned through the minimum in the measured rms width of the x-ray image or the minimum of the rms error of the long-trace profiler residual curve.

The second approach to correction of any type of spherical aberration is to apply an adjustable point load at the center of the mirror. On large mirrors this is fairly easy to do. Application of beam theory shows that the result of the point load alone is to generate a cubic shape of the general form $y = ux^2 + v|x|^3$, which means that the effect is to deliver a controlled cubic contribution. It is true that an unintended quadratic contribution is produced at the same time but this can be removed because we can add any amount of defocus using the end couples and the principle of superposition applies. Including the center load, we now have a new generic shape $y = a'x^2 + c'|x|^3 + b'x^4$. Analysis of this⁴⁶ shows that the minimum rms slope error is obtained for $a' = b'L^2/5$, $c' = -8b'L/9$ and is 6.0 times smaller than for the optimum defocus corrections alone.

The overall effect of these strategies is as follows. The best rms slope error obtainable by defocus (aberration balancing) is 0.076 units and by both defocus and a central point load is 0.0126 units. The remarkable effectiveness of the combination of these two strategies is the explanation for the excellent performance of the XPEEM condenser mirror. Such performance is being achieved in spite of an initial unit of 100 μrad of end error due to correction of unintended curvature of the substrate before bending (see Section 11.1).

9.3 Operation of the Mirror at Other Than Its Design Conjugates

Suppose initially that the mirror is installed with an incidence angle $\theta + \Delta\theta$ instead of θ and that the two end couples are then adjusted for the best possible image. This tells us that focus and coma are corrected and that the dominant aberration, which is spherical aberration is reduced by aberration balancing as described in the previous section. The dominant contribution to the end slope error will then be equal to the difference between the spherical-

aberration contributions to the slope [Equation (3)] of an (r, r', θ) ellipse and an $(r, r', \theta + \Delta\theta)$ ellipse. The expected value of the rms slope error is therefore given by

$$\frac{s_{\text{rms}}}{\Delta\theta} = 0.076 \left[\frac{a_4(r, r', \theta) - a_4(r, r', \theta + \Delta\theta)}{\Delta\theta} \right] \frac{L^3}{2}, \quad (16)$$

where a_4 is given in the Appendix. Exactly analogous expressions give the rms errors due to operation at distances other than r or r' . We choose not to approximate the bracket as a derivative because it would not be a simplification and because interesting changes of the variables are not always small enough to justify it. Equation (16) enables one to plot a relationship between s_{rms} and Δr , $\Delta r'$ or $\Delta\theta$ and thus to establish a tolerance for r , r' or θ . Because of the correction of focus and coma and the reduction of the spherical aberration, the system is surprisingly forgiving of installation errors and normal surveying tolerances are usually quite sufficient.

9.4 Manufacturing Errors

Fortunately, the most important errors involved in manufacturing the mirror substrate do not lead to a change in the position of the neutral axis and are easy to treat theoretically. Using the subscript zero to identify the intended parameters of the error-free system, we can write the flexural rigidity F (defined generically as “ EI ”) as

$$F(x) = [E_0 b_0(x) + E_1 \Delta b(x)] \left(h_0 + \frac{\Delta h}{2} + \frac{\Delta h x}{L} \right)^3 / 12,$$

where a total wedge of Δh and an extra width $\Delta b(x)$ of material of modulus E_1 have been included to represent these errors. If we also include an unintended curvature with radius R_e , the optimum values of the couples, $C + \Delta C$ and $C - \Delta C$ are now altered according to

$$C_{\text{opt}} = F(0) \left(\frac{1}{R_0} + \frac{1}{R_e} \right) \quad \Delta C_{\text{opt}} = 3F(0)La_3$$

and the resulting slope error is

$$\left. \frac{dy}{dx} - \frac{dy}{dx} \right|_0 = \int_0^x \left[\frac{C_{\text{opt}} + (2\Delta C_{\text{opt}}x')/L}{F(x')} - \frac{C + (2\Delta Cx')/L}{F_0(x')} \right] dx'.$$

Note that, given appropriate changes in the bending couples, a constant fractional error in either the width or the thickness of the substrate does not lead to errors in the final shape.

10 Mirror Materials: General Considerations

Apart from building elliptical mirrors, the ALS group also addressed some interesting materials questions associated with mirror bending. One of the requirements is always that the mirror must be joined to the bending machine. This is easy for metals, one can simply use nuts and bolts. On the other hand for ceramics (glass and silicon) it usually im-

plies the use of adhesive or solder, which raises questions of shrinkage and distortion discussed earlier. To build the μ -XPS mirrors (see Table 1), it was necessary to bend one mirror to 4.5 m radius. This is difficult for ceramics because, due to stress considerations, the thickness has to be reduced to around a millimeter, which gives insufficient rigidity for high-quality polishing. For metals, it is easy to find materials with a high stress capability, which allows the substrate to be thicker and easier to polish. On the other hand, metals do not offer a path to multilayer-coated mirrors and there are obviously risks in subjecting an electroless-nickel coating, which may have significant stresses of its own, to high bending stress.

We approached these technical challenges in two ways. First we developed the technique of superpolishing bare stainless steel.⁴⁷ The material used was a martensitic precipitation-hardening stainless steel (type 17-4 PH), which has manufacturing properties similar to commonly used alloys such as type 304, and which, upon aging at a moderate temperature, acquires a yield strength of 1.3 GPa and excellent dimensional stability (changes⁴⁸ <0.05 ppm/year). A more detailed study of the materials issues involved in the stability, polishability and other properties of this alloy are given by Howells and Casstevens.⁴⁷ The finish achieved by Dallas Optical Systems (Rockwell, Texas, 1996) on a total of 13 mirrors to date has been in the range 2 to 3 Å rms as measured by the ALS optical profiler with spatial frequency range 0.3 to 100 mm⁻¹. We believe that this ability to superpolish stainless steel could have far-reaching consequences for the design of synchrotron radiation optics generally.

Second, we have improved our technique⁴⁹ for ceramic-to-metal adhesive joints to the point where mirror distortions due to glue shrinkage have become difficult to see using our standard metrology methods. As noted, this has involved placing the joint surfaces perpendicular to the plane of the mirror (i.e., on the ends). We have also adopted some of the established practices of the aerospace industry in designing glue joints for strength.⁵⁰ In particular, we ensure that the edges of the glue layer are always in compression or shear, not tension. Furthermore, we introduce a weak link (known as a “foot”) at one end of the joint to ensure that the loads transferred to the glue at the vulnerable point are relatively small (Fig. 7). Based on considerations of strength, vapor pressure and shrinkage, our latest mirrors are being built⁴⁹ with glue type 9309.3NA made by Dexter-Hysol (Pittsburg, California, 1998).

We do not believe that there is just one optimum way to make a bent mirror. The variety of requirements encountered in synchrotron radiation practice demand that all of the material options, ceramic, metal and nickel-plated metal should be available. In the section that follows, we describe several successful mirrors that provide practical examples of the techniques discussed above. The examples are summarized in Table 1, which provides most of the parameters describing the function and performance of the mirrors. We include in the table one mirror that is not an ellipse (the 7.3.3 condenser) because it illustrates several of the technical issues we have discussed, especially the design of the end fixtures and epoxy joints⁴⁹ (Fig. 7).

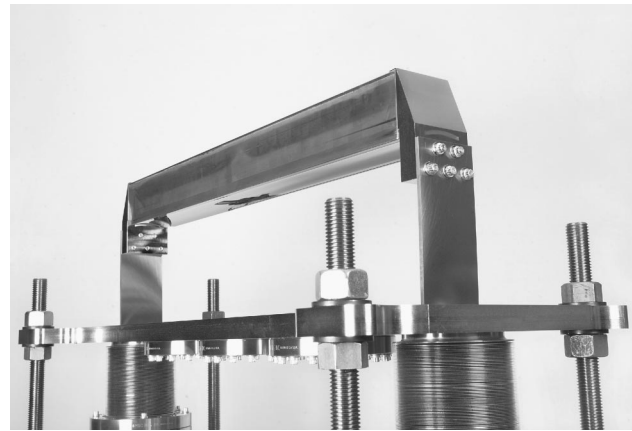


Fig. 7 The 7.3.3. condenser mirror before installation into its vacuum tank. The “foot” described in Section 10 can be seen at the top of each end plate. The x-ray beam passes through the curved slots in the end plates and reflects from the bottom surface. For descriptive and performance parameters of the mirror, see Table 1.

11 Experimental Measurements on Real Elliptical Mirrors

11.1 The XPEEM Condenser⁵¹

This mirror (shown in Fig. 15 in Section 11.3) illustrates a number of interesting points. It belongs to the class of mirrors that would suffer large errors were they to be put in tension by the bender. Therefore, a bender roughly similar to that of Fig. 3(b) was used. The large size of the mirror was to enable a large horizontal collection angle for a soft-x-ray bending magnet beam line and the goal was to produce a 10-times-demagnified image of the source. The geometrical image size was to be 30 μ m, which would define the width of the image field of the XPEEM. The choice of material was based on an approach to dimensional stability, which has been used with some success in experiments directed toward high-stability gage-blocks.⁴⁸ The strategy is to use a fully annealed, plain carbon steel with very low carbon, in this case AISI type 1006. With suitably slow heating to, and cooling from, the anneal temperature (say 2 hours/cm of section), this gives optimum stress relief. It also eliminates all of the martensite-tempering-type reactions that could lead to instability, and provides a simple low-cost substrate with a good thermal match to the electroless-nickel layer that was applied to all of the mirror surfaces. Since the material is practically pure iron, it has a much better thermal conductivity than high-alloy steels. The microyield stress will be somewhat reduced by the anneal but the moderate bending stresses required (20 MPa) can still be tolerated. The mirror suffered from an initial curvature of about 0.5 km that was not removed by either lapping or polishing. After adjusting the couples to allow for this, a marginal-ray spherical aberration of 100 μ rad was produced. This was reduced using both deliberate defocus and a point load at the center, as described in Section 9.2.2, so that the rms slope error was brought down to 14 μ rad rms over 1.1 m and 3.0 μ rad rms over 0.6 m (Fig. 8). It is also reassuring that the shape of the mirror after the two types of spherical-aberration correction (Fig. 8) was in close agreement with the calculated shapes.⁴⁶ Moreover, the measured x-ray spot width at full mirror aperture was

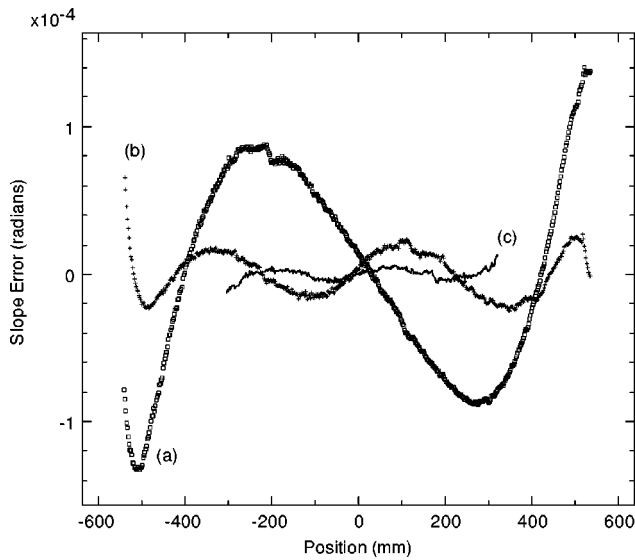


Fig. 8 Attempts to improve the XPEEM mirror surface profile as measured by the long-trace profiler. For curve (a) the rms slope error was minimized over the full length of the mirror (1.0 m) by tuning the defocus, for curve (b) the same thing was done with additional assistance from the variable point load at the center, and in curve (c) an optimization similar to that for curve (b) was applied over only the center 0.6 m.

almost exactly equal to the desired $30\ \mu\text{m}$ (Fig. 9). We conclude that, although the performance was surprisingly good for such a difficult mirror, improvements are still possible by attention to the initial preparation of the blank.

11.2 μ -XPS Mirror Pair

The mirror pair used for the μ -XPS Kirkpatrick-Baez system are described by the parameters given in Table 1. The most unusual feature is the extreme curvature which, as explained in Section 10, led us to the stainless steel substrate. The manufacturing sequence used with the successful mirrors was as follows.

1. Receive the material in the form of solution-treated bar stock, hot or cold finished.

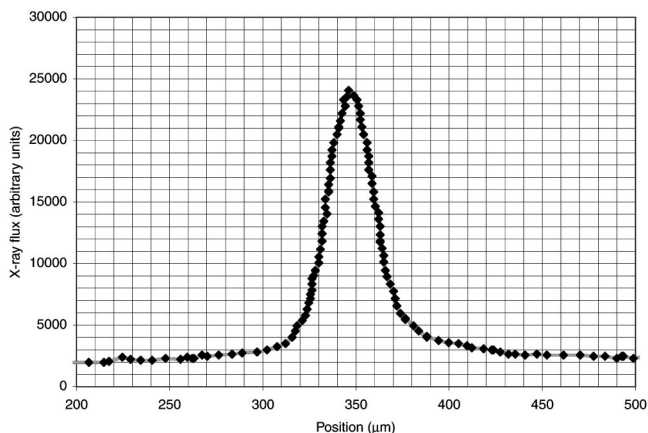


Fig. 9 XPEEM mirror x-ray spot. The intended image width of $30\ \mu\text{m}$ (the 10-times-demagnified horizontal source width of the ALS) was almost exactly achieved.

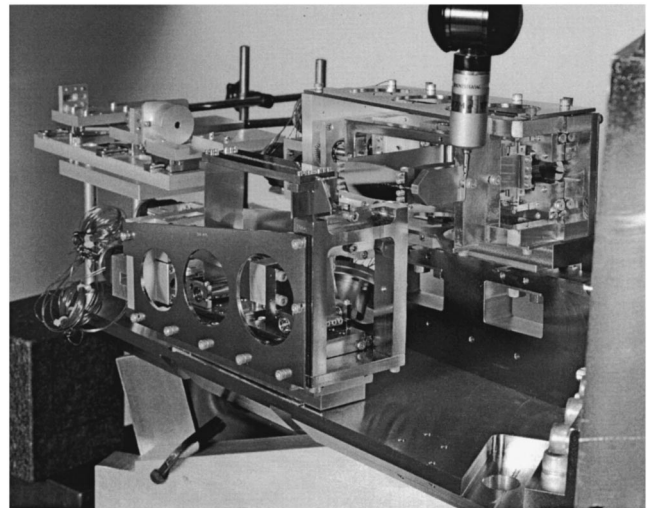


Fig. 10 μ -XPS mirror pair installed in their UHV benders. For descriptive and performance parameters of the mirrors, see Table 1.

2. Machine to size including the calculated edge shape for elliptical bending.
3. Slowly raise to 480°C , hold for 1 h, air cool.
4. Fine grind back and front surfaces to a flatness of about $1\ \mu\text{m}$.
5. Thermally cycle slowly to -196°C and 200°C , total of three cycles.
6. Lap, removing at least 20 to $30\ \mu\text{m}$ on both sides and polish.

The front of the mirror was polished⁴⁹ to the figure and finish given in Table 1 while the back was lapped to a sufficient flatness that it remained within tolerance when it was bolted to the (similarly lapped) mating surfaces of the bending springs. After due attention to assembling the bender and springs without unacceptable twisting of the mirror, the procedure described by Rah et al.²⁹ was followed to choose the values of the couples for best fidelity to the desired ellipse. The final mirror shapes followed their intended ellipses within 1 to $3\ \mu\text{rad}$, which enabled x-ray spot widths of $1 \times 1.2\ \mu\text{m}$ to be obtained at 1 keV in μ -XPS experiments. The majority of the mirror errors contributing to the spot width came from lack of flatness before bending.

The mounted pair of mirrors are shown in their ultrahigh-vacuum (UHV) bending system ready for installation in Fig. 10. The method of mounting the mirrors using a closely spaced row of bolts directly threaded into the ends of the bending springs can be clearly seen in the picture. The center bolt is reversed to enable the beam to pass. This scheme is simple and effective and did not lead to significant mirror distortions except within about one mirror thickness of the line of bolts.

11.3 μ -XRD Mirror Pair

The μ -XRD mirrors were built for hard x rays with correspondingly smaller grazing angles and less high-order optical correction.^{21–23} The quadratic and cubic approximations are at their best in this situation and in fact the edge

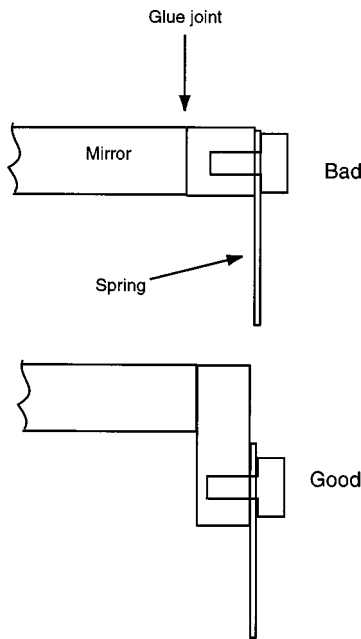


Fig. 11 Some ideas on how to isolate the stresses in the end blocks from the mirror.

function of one of the μ -XRD mirrors was approximated by three straight lines without loss of performance. The development of these mirrors taught us a good deal about how to glue metal fixtures to the mirror. In particular, the need to have the glue joint on the ends of the mirror became evident following the measurements shown in Fig. 5. However, we found that even when this is done, it is still possible to introduce unacceptable distortions if the forces due to the screws transmit excessive stresses to the mirror. The solution is to ensure that the stress pattern due to the screws is isolated from the mirror as shown in Fig. 11. Once these problems were resolved, a rms slope error of $0.8 \mu\text{rad}$ was obtained for the largest μ -XRD mirror (Fig. 12) and $0.65 \mu\text{rad}$ for the smaller, enabling a final mea-

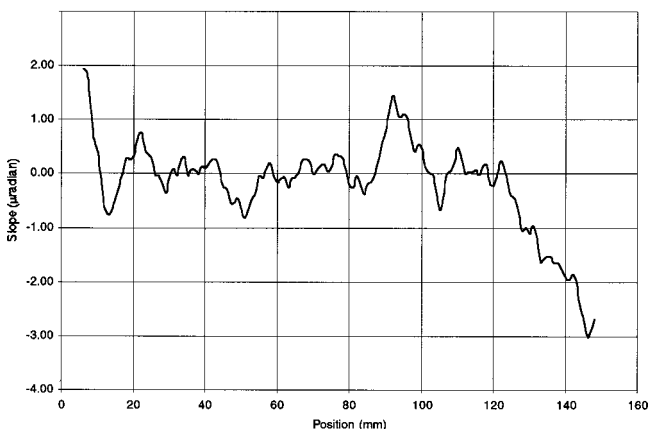


Fig. 12 Long-trace-profiler measurement of the successful μ -XRD mirror after the problems shown in Fig. 5 had been resolved. The rms slope error was $0.87 \mu\text{rad}$.

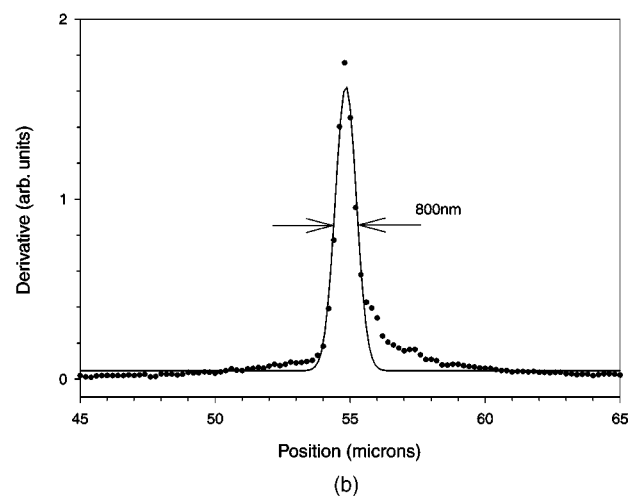
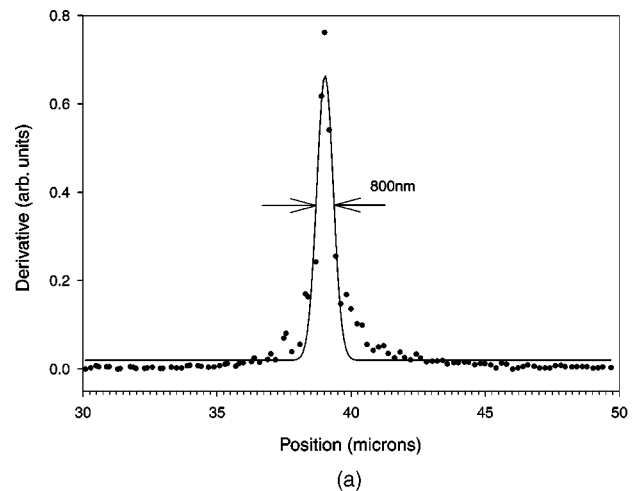


Fig. 13 X-ray spot sizes achieved by the μ -XRD mirrors in normal operation in (a) the horizontal and (b) the vertical direction.

sured x-ray spot size of $0.8 \times 0.8 \mu\text{m}^2$ (Fig. 13). (The latter image size and the others in the remainder of this section are full width at half maximum.)

The two mirrors are operated at 300:1 demagnification in the horizontal and 60:1 in the vertical. These choices reflect the actual asymmetry of the source [$300(\text{H}) \times 60(\text{V}) \mu\text{m}^2$] at the time the mirrors were designed. The present source size is $240 \times 20 \mu\text{m}^2$ so the expected image size is now $0.8 \times 0.33 \mu\text{m}^2$, which is to be compared to the observed size of $0.8 \times 0.8 \mu\text{m}^2$. Evidently the vertical spot width is slope-error-limited while the horizontal is not which still leaves unanswered the question of just how good the horizontally-focusing mirror may be. One way to test it under more challenging conditions would be to image the new smaller vertical source width. In this case, the geometrical image width is $20/300 = 0.067 \mu\text{m}$ and the diffraction limit (equal to half the wavelength divided by the numerical aperture) is $0.05 \mu\text{m}$. On the basis of the measured rms slope error of $0.65 \mu\text{rad}$ we can naively derive an image width of $0.32 \mu\text{m}$ FWHM and the quadratic sum of these three contributions is $0.33 \mu\text{m}$. The measured image width is $0.4 \mu\text{m}$ (Fig. 14), which is in good agreement with this. Thus, although the manufacturing error is still the larg-

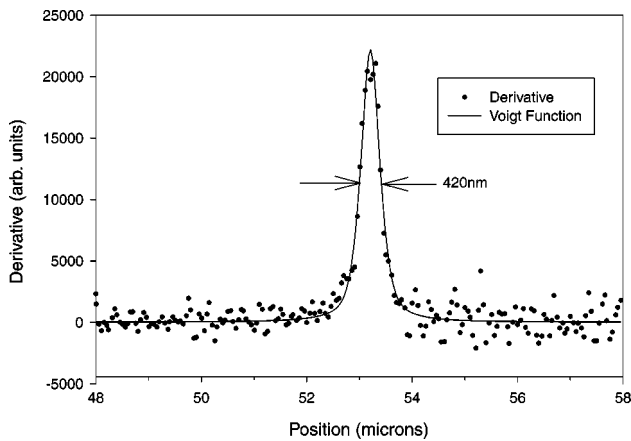


Fig. 14 Spot size of the smaller (higher demagnification) μ -XRD mirror set to image the vertical source width of 20 μm .

est contribution, the mirror performance is beginning to get within sight of the fundamental limits. The mirror used in this last measurement which is our smallest mirror to date is shown Fig. 15 together with our largest mirror, the XPEEM condenser.

12 Conclusion

We discussed the techniques by which polished flat plates can be bent to form high-quality elliptical mirrors. We reported details of actual mirrors now being used at the ALS to illustrate the principles and to show that surface accuracies better than 1 μrad rms and spot sizes better than 1 μm can be achieved using these methods. We have discussed the use of both metal and ceramic mirrors and shown that both can be used successfully. For metals, the manufacturing techniques involved are all standard machine-shop procedures, while for ceramics, metal end fixtures are glued to the mirror. We have discussed the various types of error

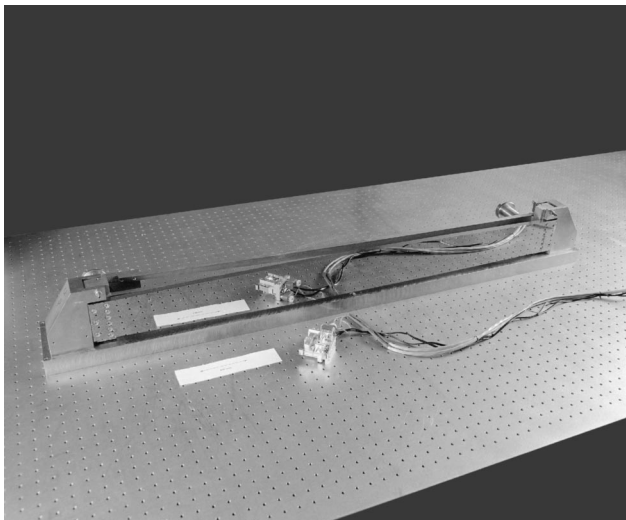


Fig. 15 Smallest μ -XRD mirror and the 1.25-m-long XPEEM condenser at the ALS optical metrology laboratory. For descriptive and performance parameters of both mirrors, see Table 1.

that can degrade the accuracy of the elliptical surface and we believe that we have a reasonable understanding of them.

The production of an elliptical cylinder surface by bending is achieved by shaping the edges of the flat mirror to a width that is calculated by beam theory. Our experience is that the small errors that we do observe are not due to a failure of this procedure but rather to lack of flatness of the mirror before bending. Thus we expect that these techniques can be improved still further by attention to the grinding-lapping-polishing procedure and to the steps involved in connecting the mirror to the bending machine.

It is still not clear where the ultimate limits to reflective microfocusing will turn out to be. We have got within a factor of 8 of the diffraction limit in one hard x-ray case (Section 11.3), which means we would be quite near the soft x-ray diffraction limit. We believe that we can close the gap still further in the future.

13 Appendix: Elliptical Mirror Expansion Coefficients

To list the coefficients a_i defined in Equation (2) as compactly as possible we adopt the following shorthand notation

$$u = \sin \theta \left(\frac{1}{r} - \frac{1}{r'} \right),$$

$$v = \frac{1}{rr'}.$$

The coefficients are then

$$a_0 = 0, \quad a_1 = 0,$$

$$a_2 = \frac{\cos \theta}{4} \left(\frac{1}{r} + \frac{1}{r'} \right), \quad a_3 = \frac{a_2 u}{2},$$

$$a_4 = a_2 \left(\frac{5u^2}{16} + \frac{v}{4} \right), \quad a_5 = a_3 \left(\frac{7u^2}{16} + \frac{3v}{4} \right),$$

$$a_6 = a_2 \left(\frac{21u^4}{128} + \frac{7u^2v}{16} + \frac{v^2}{8} \right),$$

$$a_7 = a_3 \left(\frac{33u^4}{128} + \frac{15u^2v}{16} + \frac{5v^2}{8} \right),$$

$$a_8 = a_2 \left(\frac{429u^6}{4096} + \frac{495u^4v}{1024} + \frac{135u^2v^2}{256} + \frac{5v^3}{64} \right),$$

$$a_9 = a_3 \left(\frac{715u^6}{4096} + \frac{1001u^4v}{1024} + \frac{385u^2v^2}{256} + \frac{35v^3}{64} \right),$$

$$a_{10} = a_2 \left(\frac{2431u^8}{32768} + \frac{1001u^6v}{2048} + \frac{1001u^4v^2}{1024} + \frac{77u^2v^3}{128} + \frac{7v^4}{128} \right).$$

Acknowledgments

This work was supported by the director, Office of Energy Research, Office of Basic Energy Sciences, Materials Sciences Division of the U.S. Department of Energy, under Contract No. DE-AC03-76SF00098. It is also a pleasure to acknowledge the help and advice of K. Frank, N. Hartman, L. J. Hart-Smith, G. Morrison and R. Paquin.

References

1. P. Chevallier, P. Dhez, F. Legrand, A. Erko, Y. Agafonov, L. A. Panchenko, and A. Yakshin, "The LURE-IMT x-ray fluorescence photon microprobe," *J. Trace Microprobe Tech.* **14**, 517–539 (1996).
2. J. H. Underwood, A. C. Thompson, J. B. Kortright, K. C. Chapman, and D. Lunt, "Focusing x-rays to a 1 μm spot using elastically bent, graded multilayer coated mirrors," *Rev. Sci. Instrum.* **67**, 1–5 (1996).
3. P. Dhez, P. Chevallier, and T. B. Lucatorto, "Instrumental aspects of x-ray microbeams in the range above 1 keV," *Rev. Sci. Instrum.* **70**, 1907–1920 (1999).
4. P. Kirkpatrick and A. V. Baez, "Formation of optical images by x-rays," *J. Opt. Soc. Am.* **38**, 776–774 (1948).
5. J. Underwood, Personal Communication (1991).
6. G. Lemaitre, "Optical figuring by elastic relaxation methods," in *Current Trends in Optics*, F. T. Arrecchi and F. R. Aussenegg, Eds., Taylor and Francis, London (1981).
7. W. Ehrenberg, "X-ray optics: the production of converging beams by total reflection," *J. Opt. Soc. Am.* **39**, 741–746 (1949).
8. A. Franks, *Br. J. Appl. Phys.* **9**, 349–352 (1958).
9. A. Franks and P. R. Breakwell, "Developments in optically focussing reflectors for small-angle x-ray scattering cameras," *J. Appl. Crystallogr.* **7**, 122–125 (1974).
10. D. Bilderback, C. Henderson, and C. Prior, "Elastically bent mirror for focussing synchrotron x-rays," *Nucl. Instrum. Methods Phys. Res. A* **A246**, 428–433 (1986).
11. S. M. Heald, "Applications of bent cylindrical mirrors to x-ray beams," *Nucl. Instrum. Methods Phys. Res.* **195**, 59–62 (1982).
12. J. A. Howell and P. Horowitz, "Ellipsoidal and bent cylindrical condensing mirrors for synchrotron radiation," *Nucl. Instrum. Methods* **125**, 225–230 (1975).
13. G. E. Ice and C. J. Sparks, "A simple cantilevered mirror for focusing synchrotron radiation," *Nucl. Instrum. Methods Phys. Res. A* **266**, 394–398 (1988).
14. G. E. Ice, "Controlling gravitational distortions in long synchrotron x-ray mirrors," in *Optics for High-Brightness Synchrotron Radiation Beam Lines II*, L. E. Berman and J. Arthur, Eds., *Proc. SPIE* **2856**, 157–162 (1996).
15. R. Signorato, "R and D program on multi-segmented piezoelectric bimorph mirrors at the ESRF: status report," in *Advances in Mirror Technology for Synchrotron X-ray and Laser Applications*, A. M. Khounsary, Ed., *Proc. SPIE* **3447**, 20–31 (1998).
16. J. Susini and D. Labergerie, "Compact active/adaptive x-ray mirror: bimorph piezoelectric flexible mirror," *Rev. Sci. Instrum.* **66**, 2229–2231 (1995).
17. D. Turner and J. M. Bennett, *An Elliptical Reflector Formed by Bending a Cantilever*, Imperial College (1971).
18. J. H. Underwood, "Generation of a parallel x-ray beam and its use in testing collimators," *Space Sci. Instrum.* **3**, 259–270 (1977).
19. M. Howells, "Design strategies for monolithic adjustable-radius metal mirrors," *Opt. Eng.* **34**, 410–417 (1995).
20. M. R. Howells and D. Lunt, "Design considerations for an adjustable-curvature, high-power, x-ray mirror based on elastic bending," *Opt. Eng.* **32**, 1981–1989 (1993).
21. A. A. MacDowell, R. Celestre, C.-H. Chang, K. Frank, M. R. Howells, S. Locklin, H. A. Padmore, and R. Sandler, "Progress toward submicron hard x-ray imaging using elliptically bent mirrors," *Proc. SPIE* **3152**, 126–133 (1997).
22. A. A. MacDowell, C.-H. Chang, G. M. Lamb, R. Celestre, J. R. Patel, and H. A. Padmore, "Progress toward submicron hard x-ray imaging using elliptically bent mirrors and its application," in *X-Ray Microfocusing: Applications and Techniques*, I. McNulty, Ed., *Proc. SPIE* **3449**, 137–144 (1998).
23. H. Padmore, M. R. Howells, S. Irick, T. Renner, R. Sandler, and Y.-M. Koo, "New schemes for producing high-accuracy elliptical mirrors by elastic bending," in *Optics for High-Brightness Synchrotron Radiation Beamlines II*, L. Berman and J. Arthur, Eds., *Proc. SPIE* **2856**, 145–156 (1996).
24. H. A. Padmore, C. H. Chang, M. R. Howells, A. A. MacDowell, J. R. Patel, and R. Sandler, "Progress toward submicron imaging using elliptically bent mirrors," in *Materials Manufacturing and Measurement for Synchrotron Radiation Mirrors*, P. Z. Takacs and T. W. Tonnessen, Eds., *Proc. SPIE* **3152** (1997).
25. A. Iida and K. Hirano, "Kirkpatrick-Baez optics for a sub- μm synchrotron x-ray microbeam and its applications to x-ray analysis," *Nucl. Instrum. Methods Phys. Res. B* **114**, 149–153 (1996).
26. B. X. Yang, M. Rivers, W. Schildkamp, and P. J. Eng, "GeoCARS microfocusing Kirkpatrick-Baez mirror bender development," *Rev. Sci. Instrum.* **66**, 2278–2280 (1995).
27. L. Zang, R. Hustache, O. Highnette, E. Zigler, and A. Freund, "Design optimization of flexural hinge-based bender for x-ray optics," *J. Synchrotron Radiat.* **5**, 804–807 (1998).
28. M. R. Howells and J. Hastings, "Design considerations for an x-ray microprobe," *Nucl. Instrum. Methods Phys. Res.* **208**, 379–386 (1983).
29. S. Y. Rah, S. Locklin, S. C. Irick, and M. R. Howells, "New schemes in the adjustment of bendable elliptical mirrors using a long-trace profiler," in *Materials Manufacturing and Measurement for Synchrotron Radiation Mirrors*, P. Z. Takacs and T. W. Tonnessen, Eds., *Proc. SPIE* **3152**, 112–119 (1997).
30. A. C. Ugural and S. K. Fenster, *Advanced Strength and Applied Elasticity*, Prentice Hall, Englewood Cliffs, NJ (1995).
31. M. R. Howells, J. Anspach, and J. Bender, "An assessment of approximating aspheres with more easily manufactured surfaces," *J. Synchrotron Radiat.* **5**, 814–816 (1998).
32. M. R. Howells, R. A. Paquin, "Optical substrate materials for synchrotron radiation beam lines," in *Advanced Materials for Optics and Precision Structures*, M. A. Ealey, R. A. Paquin, and T. B. Parsonage, Eds., *Proc. SPIE* **CR67**, 339–372 (1997).
33. U. Lienert, S. Hartlaub, and A. K. Freund, "Experimental shape optimization of bent crystals," in *Materials Manufacturing and Measurement for Synchrotron Radiation Mirrors*, P. Z. Takacs and T. W. Tonnessen, Eds., *Proc. SPIE* **3152**, 120–125 (1997).
34. *Tiltmeters*, Applied Geomechanics, CA (1999).
35. R. J. Roark and W. C. Young, *Formulas for Stress and Strain*, McGraw-Hill, New York (1975).
36. S. Timoshenko, *Strength of Materials Part II*, Van Nostrand, Toronto (1940).
37. S. Ferrer, M. Krisch, F. de Bergevin, and F. Zontone, "Evaluation of the anticlastic curvature of elastically bent crystals for x-ray focusing optics," *Nucl. Instrum. Methods Phys. Res. A* **311**, 444–447 (1992).
38. M. R. Howells, "Cylindrically-bent mirrors and crystals: an analysis of errors due to the anticlastic effect," Advanced Light Source Mechanical Engineering Report LSME-724, Lawrence Berkeley National Laboratory (1997).
39. V. I. Kushnir, J. P. Quintana, and P. Georgopolos, "On the sagittal focusing of synchrotron radiation with a double crystal monochromator," *Nucl. Instrum. Methods Phys. Res. A* **328**, 588–591 (1993).
40. S. Timoshenko and S. Woinowsky-Krieger, *Theory of Plates and Shells*, McGraw-Hill, New York (1959).
41. G. G. Stoney, "The tension of metallic films deposited by electrolysis," *Proc. R. Soc. London, Ser. A* **82**, 172–175 (1909).
42. P. J. Eng, M. Neville, M. L. Rivers, S. R. Sutton, "Dynamically figured Kirkpatrick Baez x-ray microfocusing optics," in *X-Ray Microfocusing: Applications and Techniques*, I. McNulty, Ed., *Proc. SPIE* **3449**, 145–156 (1998).
43. K. L. Johnson, *Contact Mechanics*, Cambridge University Press, Cambridge (1985).
44. M. M. Frocht, *Photoelasticity*, Vol. 1, Wiley, New York (1941).
45. I. S. Bowen, "The aberrations of the concave grating at large angles of incidence," *J. Opt. Soc. Am.* **23**, 313–315 (1933).
46. M. R. Howells, "Partial correction of spherical aberration in mirrors (gravitational or intrinsic) by means of deliberate defocus," Advanced Light Source Beam Line Report, LSBL-360, Lawrence Berkeley National Laboratory (1997).
47. M. R. Howells and J. Casstevens, "Achievement of a superpolish on bare stainless steel," in *Materials, Manufacturing and Measurement for Synchrotron Radiation Mirrors*, P. Z. Takacs and T. W. Tonnessen, Eds., *Proc. SPIE* **3152**, 35–40 (1997).
48. M. R. Meyerson, P. M. Giles, P. F. Newfield, "Dimensional stability of gage block materials," *J. Mater. JMSA* **3**, 727–743 (1968).
49. N. Hartman, P. A. Heimann, A. A. MacDowell, K. D. Frank, A. Grieshop, S. C. Irick, and H. A. Padmore, "Design, analysis, and performance of an epoxy-bonded bendable mirror," in *Advances in Mirror Technology for Synchrotron X-ray and Laser Applications*, A. M. Khounsary, Ed., *Proc. SPIE* **3447**, 40–51 (1998).
50. L. J. Hart-Smith, "Stress analysis (of adhesively bonded joints): a continuum mechanics approach," in *Developments in Adhesives-2*, A. J. Kinloch, Ed., Applied Science Publishers, London (1981).
51. T. R. Renner, K. Frank, M. Howells, S. Irick, H. A. Padmore, and S.-Y. Rah, "Construction and performance of a one meter long elliptically bent steel mirror," in *Materials, Manufacturing and Measurement for Synchrotron Radiation Mirrors*, P. Z. Takacs and T. Tonnessen, Eds., *Proc. SPIE* **3152**, 17–26 (1997).



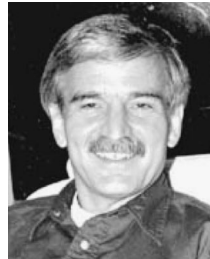
Malcolm R. Howells obtained his BA in physics from Oxford University in 1964 and his PhD in physics from London University in 1971. He began working with synchrotron radiation in 1971 and since then has been a user and/or a facility builder at six synchrotron radiation facilities. His specializations are soft x-ray imaging, especially via x-ray holography, and beam-line instrumentation such as the optical and mechanical design of x-ray mirrors and monochromators.



Howard A. Padmore received his BSc in 1977 and his PhD 1980, both from Leices-ter University. He has worked in synchro- tron radiation facilities since 1982, first at Daresbury (United Kingdom) and, since 1993, at the Advanced Light Source at Ber- keley where he heads the Experimental Systems Group. His research interests in- clude the development of microfocusing optics for hard x-ray spectroscopy and dif- fraction and their application to thin-film materials science.



Daniela Cambie obtained a DrEng degree in aerospace engineering from Milan Poly-technic, Italy, in 1997. She joined the syn- chrotron radiation field in 1998 studying cooling methods for x-ray mirrors and she joined the Advanced Light Source at Lawrence Berkeley Lab in 1999 where she is currently working on the analysis and de- sign of beam-line components in the me- chanical engineering group.



Timothy R. Renner (1950–1998) received his BSc from the University of Texas at Austin in 1972 and his PhD from the Uni- versity of Chicago in 1978. He worked in the Nuclear Science Division of the Lawrence Berkeley National Laboratory on instrumentation for particle-beam treat- ments of cancers especially of the eye. A major treatment center for such cancers at the University of California at Davis is named in his honor. He joined the Ad- vanced Light Source Division in 1993 and was responsible for sev- eral beam-line projects there including an advanced small-spot Electron Spectroscopy for Chemical Analysis (ESCA) system for In- tel Corporation.

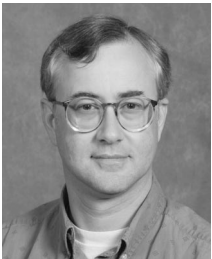


Robert M. Duarte received his BS in me- chanical engineering from the University of California, Berkeley in 1996. He has been working for the Advanced Light Source at Lawrence Berkeley National Laboratory Mechanical Engineering Department since 1990. He is currently working on beam-line projects with the Experimental Systems Group at the ALS.



Seungyu Rah received his BS degree in physics from Chonnam National University in 1984 and his MS and PhD degrees from Korea Advanced Institute of Science and Technology in 1986 and 1989, respec- tively. Since 1989, he has been a staff sci- entist with Pohang Accelerator Laboratory, Pohang Institute of Science and Technol- ogy, Korea. His research field is the design and testing of optical instruments for syn- chrotron applications. He is also interested

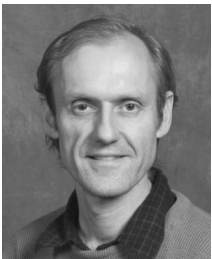
in design of reflective optical systems.



Steven Irick received his BS degree in physics and his MSME degree in applied optics, both from Purdue University. He has experience in the fields of computer generated holography, xerography, laser scanning and spectrometry. Currently he is involved with metrology of mirror surfaces for x-ray beam lines.



Reubin Sandler obtained his BS in me- chanical engineering at the University of California, Berkeley, in 1997 and his MS in 1999. He was a student employee with the Advanced Light Source where his efforts focused on mirror bender design, assem- bly, testing, and analysis. He is now a me- chanical design engineer at Berkeley Pro- cess Control in Richmond, California.



Alasdair A. Macdowell received his BSc and PhD degrees in physical chemistry from the University of Manchester in 1976 and 1980, respectively. He has worked in the development and application of various instrumental techniques used at the sev- eral synchrotron facilities he has worked at, Daresbury (United Kingdom), Brookhaven (United States) and now Berkeley (United States). His current interest is the devel- opment of x-ray absorption spectroscopy and

x-ray diffraction when operating at the micrometer spatial scale.